Journal of Applied Mechanics and Technical Physics, No. 4, 1994

NUMERICAL SIMULATION OF COMBINED HEAT TRANSFER IN A PLANAR LAYER ON A NET HAVING AN ARBITRARY THICKNESS STEP

V. P. Zamuraev

UDC 536.24

In many treatments, one needs to incorporate processes occurring at various rates and having various time or spatial scales. A good example is shock-wave structure [1]. To establish equilibrium in the translational degrees of freedom, each molecule must make two or three collisions, while dozens of collisions are required (under normal conditions) to attain equilibrium in the rotational degrees of freedom, and many more for the vibrational degrees of freedom (thousands or hundreds of thousands at about 1000 K). A similar situation occurs in the flow of a chemically reacting medium when one incorporates energy transfer by radiation.

The following approaches can be employed in simulating such cases. One involves using models in which the rates of some processes are taken as infinitely great, while other processes are considered as frozen, and one calculates only for processes whose rates do not differ greatly. This leaves open the question of the fit to the actual case. In another approach, one uses a calculation net corresponding to the fastest process. Then one has problems over run time and memory, while the accuracy remains an open question. One can also use different nets, one for each process.

Interest attaches to using a coarse net corresponding to the slowest process and correcting for the fast processes. That approach is considered here in the examination of energy transport simultaneously by convection, thermal conduction, and radiation.

The spectral attenuation coefficient often varies greatly with frequency. A medium transparent at one frequency may be optically dense at another. If the optical thickness for the spatial step in the net is of the order of or greater than one, there may be unsatisfactory accuracy in calculating the temperature pattern [2, 3]. The stability of the numerical solution also comes in question.

In the 1960s, I proposed a method of considering radiative-conductive heat transfer in a planar layer on a net having a large optical thickness for the step. Only absorption and inherent radiation from the medium were considered. That method has been used to calculate the radiative cooling of air behind strong shock waves [4, 5]. This is now extended to a radiative, absorbing, and scattering medium.

The topic has been considered by others. A method of numerical solution has been given [6] for the nonstationary transport equation in a planar layer, which is applicable to optically coarse nets [7]. In [8], the method was extended to incorporate motion of the medium with spherical symmetry. The [6] method involves detailed solution of the transport equation and then integration of the radiation intensity with respect to solid angle. Astrophysical treatments [9] concern the angular intensity distribution. In some cases in gas dynamics, there is no need for a detailed solution to the transport equation. In [7, 10], the [6] method was adapted to equations describing radiation transport in a first approximation in the spherical harmonic method (in the diffusion approximation). The numerical method proposed below enables one to avoid detailed solution of the transport equation but is based on equations accurate under certain conditions.

The method has been devised for a planar layer but can be used approximately for a boundary layer, for flow and heat transfer in a channel, for high-current arcs, and so on. The [11] data indicate the error when one uses the planar-layer approximation for a boundary layer. Isolated results from the present research have been published in [12, 13].

The following is the radiation transport equation for a planar layer showing emission, absorption, and scattering [2]:

Novosibirsk. Translated from Prikladnaya Mekhanika i Tekhnicheskaya Fizika, No. 4, pp. 107-118, July-August, 1994. Original article submitted August 30, 1993.

0021-8944/94/3504-0584$12.50

$$\mu\frac{\partial J(\tau,\mu)}{\partial\tau} + J(\tau,\mu) = f = (1-\omega)n^2J^0(\tau) + \frac{1}{2}\omega\int_{-1}^{1}J(\tau,\mu')\gamma(\mu,\mu')d\mu', \tag{1}$$

in which $J(\tau, \mu)$ is the spectral radiation intensity, $\tau = \int_0^y k(y')dy'$, the optical thickness, y the coordinate transverse to the layer; $\mu = \cos\theta$; θ, the angle between the radiation direction and the y axis, J^0, the Planck function, k the attenuation coefficient, which equals the sum of the absorption and scattering coefficients; ω, the single-scattering albedo; and n, the refractive index. An expansion in terms of Legendre polynomials containing a finite number of terms is used for the scattering indicatrix, which takes the following form for a planar layer with allowance for integration with respect to the azimuthal angle:

$$\gamma(\mu,\mu') = \sum_{s=0}^{l}a_sP_s(\mu)P_s(\mu'),\ a_0 = 1. \tag{2}$$

It is assumed that the boundaries of the layer radiate and reflect diffusely, so

$$\begin{aligned} J(0,\mu) &= \varepsilon_0n^2J^0(0) - 2r_0\int_{-1}^{0}J(0,\mu')\mu'd\mu',\ \mu > 0,\\ J(\tau_m,\mu) &= \varepsilon_mn^2J^0(\tau_m) + 2r_m\int_{0}^{1}J(\tau_m,\mu')\mu'd\mu',\ \mu < 0 \end{aligned} \tag{3}$$

(ε and r are the spectral degree of blackness and spectral reflection coefficient of the corresponding boundary).

The (1)-(3) problem reduces to a system of $l + 3$ linear integral algebraic equations. The formal solution to (1) is written as the preliminary step:

$$\begin{aligned} J(\tau,\mu) &= J(0,\mu)\exp(-\tau/\mu) + \int_0^{\tau}f(\tau',\mu)\exp(-(\tau-\tau')/\mu)d\tau'/\mu,\ \mu > 0,\\ J(\tau,\mu) &= J(\tau_m,\mu)\exp((\tau_m-\tau)/\mu) - \int_{\tau}^{\tau_m}f(\tau',\mu)\exp(-(\tau-\tau')/\mu)d\tau'/\mu, \end{aligned} \tag{4}$$

We introduce the intensity moments:

$$M_r(\tau) = 2\pi\int_{-1}^{1}J(\tau,\mu)P_r(\mu)d\mu. \tag{5}$$

The moment for r = 0 is the product of the velocity of light and the radiation energy density, while it is the radiation flux for r = 1. Equations (4) are multiplied by $P_r(\mu)$, integrated with respect to the corresponding values of μ, and are added. With (2) we get a system of $l + 1$ linear integral equations for the (5) moment $l = 1$:

$$\begin{aligned} M_r(\tau) = J_0Z_{r1}(\tau) + (-1)^rJ_mZ_{r1}(\tau_m-\tau) + \sum_{s=0}^{l}\Big(\int_0^{\tau}\varphi_s(\tau')Z_{rs}(\tau-\tau')d\tau' +\\ + (-1)^{r+s}\int_{\tau}^{\tau_m}\varphi_s(\tau')Z_{rs}(\tau'-\tau)d\tau'\Big),\ r = 0, 1, ..., l. \end{aligned} \tag{6}$$

Here

$$\begin{aligned} &J_0 = 2\pi J(0,\mu)\ (\mu > 0);\ J_m = 2\pi J(\tau_m,\mu)\ (\mu < 0);\\ &\varphi_0 = 2\pi(1-\omega)n^2J^0 + \frac{1}{2}\omega M_0;\ \varphi_s = \frac{1}{2}\omega a_sM_s\ (s = 1, ..., l);\\ &Z_{rs}(\tau) = \int_0^1\exp(-\tau/\mu)P_r(\mu)P_s(\mu)d\mu/\mu. \end{aligned}$$

The functions $Z_{rs}(\tau)$ are expressed in terms of integroexponential functions, e.g., $Z_{00}(\tau) = E_1(\tau)$, $Z_{01}(\tau) = E_2(\tau)$, $Z_{11}(\tau) = E_3(\tau)$. In the general case

$$Z_{rs}(\tau) = \frac{1}{2^{r+s}}\sum_{i=0}^{E(r/2)}\sum_{j=0}^{E(s/2)}\frac{(-1)^{i+j}(2r-2i)!(2s-2j)!}{i!(r-i)!(r-2i)!j!(s-j)!(s-2j)!}\times E_{r+s-2(i+j)+1}(\tau),$$

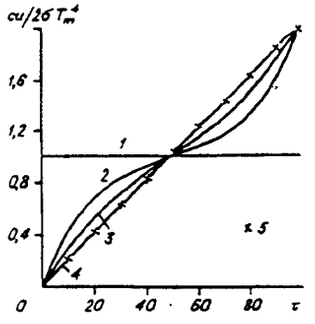

Fig. 1

where the upper limit in the summation is the integer part of the fraction.

Equations (6) have been written on the basis that the radiation from the layer boundaries is isotropic. J_0 and J_m are derived from the (3) boundary conditions, which expressed in terms of the intensity moments are

$$\begin{aligned} \varepsilon_0(J_0 - 2n^2\pi J^0(0)) + 2(1 - \varepsilon_0)M_1(0) = 0, \\ \varepsilon_m(J_m - 2n^2\pi J^0(\tau_m)) - 2(1 - \varepsilon_m)M_1(\tau_m) = 0. \end{aligned} \tag{7}$$

There is a difference from the standard spherical harmonic method, where the unknown quantities are also the intensity moments, in that one obtains system (6) and (7) in this approach as one close for finite l (the number of equations is equal to the number of unknown quantities). The solution gives the moments up to order l. If necessary, one can also determine higher-order moments. For that purpose, (6) should be supplemented with the corresponding equations. Each new equation introduces one new unknown quantity. If some of the coefficients in the (2) expansion for the scattering indicatrix are zero: $a_s = 0$, $0 < s < l$, then the (6) equations for the moments with the same indices need not be considered, an exception being the case $a_1 = 0$ with diffuse reflection from the boundary surface, since M_1 with that type of reflection influences the other intensity moments via the (7) boundary conditions. If there is specular reflection, the corresponding boundary condition can be satisfied in that method only approximately.

The numerical solution to (6) and (7) is derived as in [3] by means of the net $\tau = \tau_i$ (i = 0, 1, ..., m), $\tau_0 = 0$. The step in the net $\Delta\tau_i = \tau_i - \tau_{i-1}$ in general is variable. The (6) equations are written at the nodes. The factors $\varphi_s(\tau)$ in the integrands are approximated at each step by means of a linear function of τ, and for even (r + s) in the steps adjacent to the working point by means of a quadratic function. The (6) equations for the nodes at the boundaries of the region have the $\varphi_s(\tau)$ factors approximated in the steps adjoining the boundaries in all cases by a quadratic function. Then the (6) equations reduce to a system of linear algebraic equations:

$$\begin{aligned} M_{ri} = J_0 Z_{r1}(\tau_i) + (-1)^r J_m Z_{r1}(\tau_m - \tau_i) + \sum_{s=0}^{l} (-\varphi_{s0} Y''_{rs}(\tau_i) \\ - (-1)^{r+s}\varphi_{sm} Y''_{rs}(\tau_m - \tau_i) + (1 + (-1)^{r+s})\varphi_{si} Y''_{rs}(0) \\ + \sum_{j=1}^{i} \psi_{sj}(Y'_{rs}(\tau_i - \tau_j) - Y'_{rs}(\tau_i - \tau_{j-1})) \\ + (-1)^{r+s} \sum_{j=i+1}^{m} \psi_{sj}(Y'_{rs}(\tau_j - \tau_i) - Y'_{rs}(\tau_{j-1} - \tau_i)) + \Delta_{rsi}), \\ r = 0, 1, ..., l, \; i = 0, 1, ..., m. \end{aligned} \tag{8}$$

Here $M_{ri} = M_r(\tau_i)$; $\varphi_{si} = \varphi_s(\tau_i)$; $\psi_{sj} = \Delta\varphi_{sj}/\Delta\tau_j$; $Y''_{rs}(\tau) = -Z_{rs}(\tau)$; a prime denotes differentiation with respect to the argument, and Δ_{rsi} are additional terms related to the quadratic approximation for the $\varphi_s(\tau)$ functions:

$$\Delta_{rsi} = \delta_{rs}(\psi_{s,i+1} - \psi_{si})(e_{rsi} + (-1)^{r+s}e_{rs,i+1})/(\Delta\tau_i + \Delta\tau_{i+1}),$$
$$i = 1, \ldots, m-1,$$
$$\Delta_{rs0} = (\psi_{s1} - \psi_{s1})e_{rs1}/\tau_2, \Delta_{rsm} = (\psi_{sm} - \psi_{s,m-1})e_{rsm}/(\Delta\tau_m + \Delta\tau_{m-1}),$$
$$e_{rsi} = 2(Y_{rs}(0) - Y_{rs}(\Delta\tau_i)) + \Delta\tau_i(Y'_{rs}(0) + Y'_{rs}(\Delta\tau_i)),$$
$$\delta_{rs} = \frac{1}{2}(1 + (-1)^{r+s}).$$

This difference approximation for (6) giving the M_r moments satisfies the limiting approximations for the optically thin and thick cases:

$$\tau_m \to 0: M_{ri} \to (J_0 + (-1)^r J_m)Z_{r1}(0),\ i = 0, 1, \ldots, m,$$
$$\Delta\tau \to \infty: M_{ri} \to \sum_{s=0}^{i}((1 + (-1)^{r+s})(\varphi_{si}Y''_{rs}(0)$$
$$+ \frac{1}{2}(1 + (-1)^{r+s})\varphi''_{si}Y_{rs}(0)) + (1 - (-1)^{r+s})\varphi'_{si}\ Y'_{rs}(0)),$$
$$i = 1, \ldots, m-1,$$
$$M_{r0} \to J_0 Z_{r1}(0) + \sum_{s=0}^{i}(-1)^{r+s}(\varphi_{s0}Y''_{rs}(0) - \varphi'_{s0}Y'_{rs}(0) + \varphi''_{s0}Y_{rs}(0)),$$
$$M_{rm} \to (-1)^r J_m Z_{r1}(0) + \sum_{s=0}^{i}(\varphi_{sm}Y''_{rs}(0) + \varphi'_{sm}Y'_{rs}(0) + \varphi''_{sm}Y_{rs}(0)).$$

The coefficient δ_{rs} in the expression for Δ_{rsi} could be taken as one for any s, which does not affect the error in approximating the equations. On the other hand, the equations written for the internal nodes and for the nodes at the boundaries of the region agree best one with another. However, the computational algorithm becomes somewhat more complicated.

One adds (7) to system (8), which with these symbols becomes

$$\begin{aligned}\varepsilon_0(J_0 - n^2\pi J_0^0) + (1 - \varepsilon_0)M_{10} = 0,\\ \varepsilon_m(J_m - n^2\pi J_m^0) - (1 - \varepsilon_m)M_{1m} = 0.\end{aligned} \tag{9}$$

The system of $N = (m + 1)(l + 1) + 2$ linear algebraic equations in (8) and (9) includes the N unknown quantities M_{ri} ($r = 0, 1, \ldots, l$, $t = 0, 1, \ldots, m$), J_0, J_m, and it can be solved by standard methods. Here I propose the following method. We distinguish on the right-hand sides of the (8) equations the terms dependent on the intensity moments M_{sj} ($s = r$, $j = i - 1, i, i + 1$), which determine the contributions for $s = r$ to the limiting approximations for M_{ri}. These terms are combined into groups denoted by $\Phi 1_{ri}$:

$$\Phi 1_{ri} = 2\varphi 1_{ri}Y''_{rr}(0) - \varphi 1_{r,i-1}Y''_{rr}(\Delta\tau_i) - \varphi 1_{r,i+1}Y''_{rr}(\Delta\tau_{i+1})$$
$$+ \frac{\Delta\varphi 1_{ri}}{\Delta\tau_i}(Y'_{rr}(0) - Y'_{rr}(\Delta\tau_i)) + \frac{\Delta\varphi 1_{r,i+1}}{\Delta\tau_{i+1}}(Y'_{rr}(\Delta\tau_{i+1})$$
$$- Y'_{rr}(0)) + \left(\frac{\Delta\varphi 1_{r,i+1}}{\Delta\tau_{i+1}} - \frac{\Delta\varphi 1_{ri}}{\Delta\tau_i}\right)(e_{rri} + e_{rr,i+1})/(\Delta\tau_i + \Delta\tau_{i+1}),$$
$$i = 1, \ldots, m-1,$$
$$\Phi 1_{r0} = \varphi 1_{r0}Y''_{rr}(0) - \varphi 1_{r1}Y''_{rr}(\Delta\tau_1) + \frac{\Delta\varphi 1_{r1}}{\Delta\tau_1}(Y'_{rr}(\Delta\tau_1) - Y'_{rr}(0)) + \left(\frac{\Delta\varphi 1_{r2}}{\Delta\tau_2} - \frac{\Delta\varphi 1_{r1}}{\Delta\tau_1}\right)e_{rr1}/\tau_2,$$
$$\Phi 1_{rm} = \varphi 1_{rm}Y''_{rr}(0) - \varphi 1_{r,m-1}Y''_{rr}(\Delta\tau_m) + \frac{\Delta\varphi 1_{rm}}{\Delta\tau_m}(Y'_{rr}(0) - Y'_{rr}(\Delta\tau_m))$$
$$+ \left(\frac{\Delta\varphi 1_{rm}}{\Delta\tau_m} - \frac{\Delta\varphi 1_{r,m-1}}{\Delta\tau_{m-1}}\right)e_{rrm}/(\Delta\tau_m + \Delta\tau_{m-1}),\ r = 0, 1, \ldots, l.$$

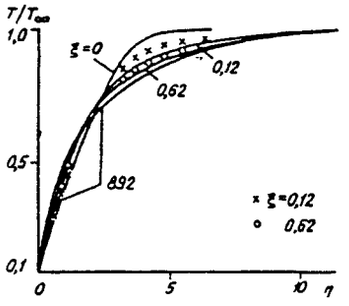

Fig. 2

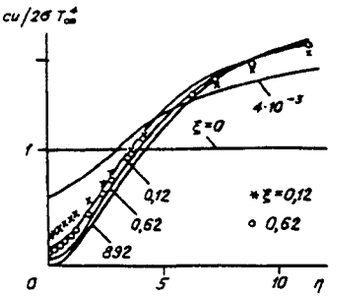

Fig. 3

Here $\varphi 1_{0i} = 1/2\omega M_{0i}$; $\varphi 1_{si} \equiv \varphi_{si}$ (s = 1, ..., l). All the other terms on the right in (8) form the $\Phi 2_{ri}$ groups. One then has the following successive-approximation scheme for solving (8):

$$M_{ri}^{(s+1)} = \Phi 1_{ri}^{(s+1)} + \Phi 2_{ri}^{(s,s+1)}, \; r = 0, 1, ..., l, \; i = 0, 1, ..., m.$$

These equations become

$$\begin{aligned} a_{r0}M_{r2}^{(s+1)} - b_{r0}M_{r1}^{(s+1)} + c_{r0}M_{r0}^{(s+1)} + d_{r0} &= 0, \\ a_{ri}M_{r,i+1}^{(s+1)} - b_{ri}M_{ri}^{(s+1)} + c_{ri}M_{r,i-1}^{(s+1)} + d_{ri} &= 0, \; i = 1, ..., m-1, \\ a_{rm}M_{rm}^{(s+1)} - b_{rm}M_{r,m-1}^{(s+1)} + c_{rm}M_{r,m-2}^{(s+1)} + d_{rm} &= 0, \; r = 0, 1, ..., l. \end{aligned} \tag{10}$$

System (8) as it were splits up into $l + 1$ subsystems. Each of these subsystems is characterized by a certain value of r and has a matrix that can readily be reduced to three-diagonal form by eliminating M_{r2} and $M_{r,m-2}$ correspondingly from the first and last equations in (10) by means of the equations for i = 1 and i = m − 1. This means that the pivot method can be used in solving (10).

The following explanation is required here. When one calculates $d_{ri} = \Phi 2_{ri}^{(s,s+1)}$, the moments of order r are taken from the previous approximation (with number s), while the moments of order different from r already derived in approximation s + 1 can be used in that approximation. The order in which the moments are calculated may be important. It would be more logical to distinguish all the terms on the right in (8) that determine the contributions in the limiting cases and write those terms in approximation s + 1, while the others are written in approximations s and then one applies matrix pivot fitting.

A numerical experiment was performed to examine the convergence: I calculated isotropic scattering in a planar layer having absolutely black boundaries. The optical thickness of the layer varied from about 0.3 to about 500. The zeroth approximation for the integral radiation density u was provided by the distribution in a layer having optical thickness zero. The calculations were performed with a uniform net, and the coordinate transverse to a layer was split up into 20 steps. Figure 1 shows results for u and for an optical thickness of the layer $\tau_m = 100$ (values of u referred to $2\delta T^4_m/c$), with $T_0 = 0.1\ T_m$, $\omega = 1$. Line 1 shows the zeroth approximation, while lines 2 and 3 show the first and second ones, with points 5 showing the calculation with a local error of 1% (seventh approximation). In that figure, the latter results merge with the values obtained with an error of 0.1% (tenth approximation, line 4). The numerical experiment confirmed the expected rapid convergence to the exact solution.

For linear anisotropic scattering, I first calculated the distribution for the first moment in the layer, which was then used to calculate the values of the zeroth moment. The successive approximations were repeated. That procedure with $\omega = a_1 = 1$ in the limit $\Delta\tau \gg 1$ ($\Delta\tau$ = const) corresponds to the successive−approximation scheme

$$M_{0,i+1}^{(s+1)} - 2M_{0i}^{(s+1)} + M_{0,i-1}^{(s+1)} - \frac{1}{2}\Delta\tau(M_{1,i+1}^{(s+1)} - M_{1,i-1}^{(s+1)}) = 0,$$

$$M_{1,i+1}^{(s+1)} - 2(1 + \frac{5}{3}\Delta\tau^2)M_{1i}^{(s+1)} + M_{1,i-1}^{(s+1)} - \frac{5}{6}\Delta\tau(M_{0,i+1}^{(s)} - M_{0,i-1}^{(s)}) = 0.$$

It is simple to show that this is stable for any $\Delta\tau$.

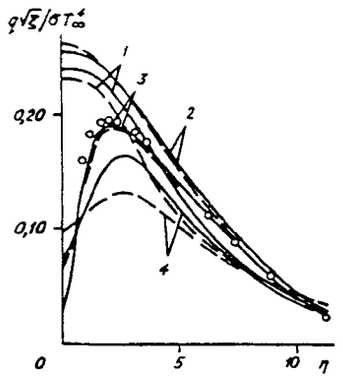

Fig. 4

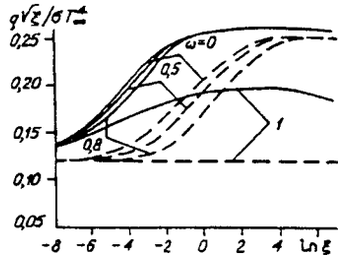

Fig. 5

System (6) should be solved together with the energy equation, so the next necessary step is to construct the difference analog of the energy equation, which should have correct results in the limiting cases of optically thin and thick layers. One is concerned primarily with the difference approximation for the radiation flux divergence, which may be written as

$$\mathrm{div}q_{\nu} = \int kQd\nu, \tag{11}$$

in which the integration is with respect to frequency, while for Q one derives an expression from (1) by integrating it with respect to solid angle: $Q = (1 - \omega)(4\pi n^2 J^0 - M_0)$. If we now use (6) for M_0, then

$$Q = (\varphi_0(\tau) - J_0)E_2(\tau) + (\varphi_0(\tau) - J_m)E_2(\tau_m - \tau)$$
$$- \sum_{s=1}^{l}\left(\int_0^{\tau} \varphi_s(\tau')Z_{0s}(\tau - \tau')d\tau' + (-1)^s\int_{\tau}^{\tau_m}\varphi_s(\tau')Z_{0s}(\tau' - \tau)d\tau'\right)$$
$$- \int_0^{\tau_m}(\varphi_0(\tau') - \varphi_0(\tau))E_1(|\tau - \tau'|)d\tau'.$$

The corresponding difference analog is derived from (8):

$$Q_i = (\varphi_{00} - J_0)E_2(\tau_i) + (\varphi_{0m} - J_m)E_2(\tau_m - \tau_i) - \sum_{s=1}^{l}[-\varphi_{s0}Y''_{0s}(\tau_i)$$
$$- (-1)^s\varphi_{sm}Y''_{0s}(\tau_m - \tau_i) + (1 + (-1)^s)\varphi_{si}Y''_{0s}(0) + \sum_{j=1}^{i}\psi_{sj}(Y'_{0s}(\tau_i - \tau_j)$$
$$- Y'_{0s}(\tau_{i,i} - \tau_{j-1})) + (-1)^s\sum_{j=i+1}^{m}\psi_{sj}(Y'_{0s}(\tau_j - \tau_i) - Y'_{0s}(\tau_{j-1} - \tau_i)) \tag{12}$$
$$+ \Delta_{0si}] + \sum_{j=1}^{m}\psi_{0j}(E_3(|\tau_i - \tau_j|) - E_3(|\tau_i - \tau_{j-1}|))$$
$$- (\psi_{0,i+1} - \psi_{0i})(e_{00i} + e_{00,i+1})/(\Delta\tau_i + \Delta\tau_{i+1}).$$

Equations (11) and (12) approximate the radiation-flux divergence, including for optically dense media.

Further, Q is represented as Q = Q1 + Q2, where

$$Q2_i = \varphi 2_{i-1}E_2(\Delta\tau_i) + \varphi 2_{i+1}E_2(\Delta\tau_{i+1}) - \frac{\Delta\varphi 2_i}{\Delta\tau_i}E_3(\Delta\tau_i) + \frac{\Delta\varphi 2_{i+1}}{\Delta\tau_{i+1}}E_3(\Delta\tau_{i+1})$$
$$- \left(\frac{\Delta\varphi 2_{i+1}}{\Delta\tau_{i+1}} - \frac{\Delta\varphi 2_i}{\Delta\tau_i}\right)e_i,$$
$$\varphi 2 = 2\pi(1 - \omega)n^2J^0,\ e_i = (e_{00i} + e_{00,i+1})/(\Delta\tau_i + \Delta\tau_{i+1}) + 1/2.$$

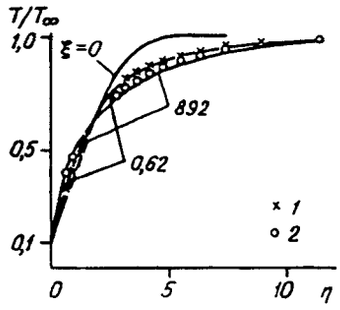

Fig. 6

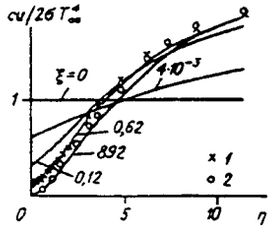

Fig. 7

The expression for $Q2_i$ includes terms related to the inherent radiation from the medium at points i − 1, i, and i + 1. Those terms provide correct values for Q_i in the radiative thermal conduction approximation. For an optically thin layer (in the limit), $Q2_i$ becomes zero.

The Planck junction J^0 in the expression for $Q2_i$ is linearized with respect to the small temperature difference $\Delta\tau_i = T_{i,s+1} - T_{is}$ in two successive approximations for the one-dimensional stationary case (or at two successive instants for nonstationary heat transfer, or between two adjacent sections of the boundary layer, and so on): $J_{i,s+1}{}^0 = J_{is}{}^0 + (dJ^0/dT)_{is}\Delta T_i$. All the other quantities in Q2 and also Q1 are calculated from the temperature profile in the preceding approximation (with number s).

That approximation for the radiation term in the energy equation provides difference sachems stable for any optical thicknesses in the spatial step. In the present case, the integrodifferential energy equation is replaced by an algebraic-equation system:

$$at_i\Delta T_{i+1} - bt_i\Delta T_i + ct_i\Delta T_{i-1} + dt_i = 0 \quad (i=1,\ldots,m-1),$$
$$\Delta T_0 = \Delta T_m = 0. \tag{13}$$

Here

$$at_i = a_i - \int k_i' g_{i+1}' au_i dv;\ bt_i = b_i - \int k_i' g_i' bu_i dv;$$
$$ct_i = c_i - \int k_i' g_{i-1}' cu_i dv;\ dt_i = d_i + \int (k(1-\omega))_i' (M_0^{(s+1)}$$
$$- 4\pi(n^2 J^0)_i') dv;$$

with a_i, b_i, c_i, and d_i defined by approximating the differential terms in accordance with an inexplicit scheme, and

$$g = 2\pi(1-\omega)n^2(dJ^0/dT);\ au_i = E_2(\Delta\tau_{i+1}) - h1;\ bu_i = h1 + h2;$$
$$cu_i = E_2(\Delta\tau_i) - h2;\ h1 = (e_i - E_3(\Delta\tau_{i+1}))/\Delta\tau_{i+1};$$
$$h2 = (e_i - E_3(\Delta\tau_i))/\Delta\tau_i.$$

This system is solved by the pivot method. The unknown temperatures are calculated from $T_{is+1} = T_{is} + \Delta T_i$.

The method was tested on radiative-conductive heat transfer in a laminar boundary layer on a flat plate. As we were concerned mainly with methods, various simplifying assumptions were made. In particular, the product of the density ρ and the viscosity was taken as constant. In that case the hydrodynamic and thermal treatments separate for the variables $\xi = x$, $\eta = 1/\sqrt{x}\int_0^y \rho dy$ (x is the coordinate along the plate as referred to a certain characteristic dimension l, with y the coordinate transverse to it as measured in terms of $\delta = l/\sqrt{Re}$, and Re is the Reynolds number). The flow was described by the dimensionless current function $f(\eta)$ defined by the solution to the Blasius treatment [14].

The energy equation is as follows with the boundary conditions written in terms of those variables:

$$\frac{\partial^2 T}{\partial\eta^2} + \frac{1}{2}f\frac{\partial T}{\partial\eta} - N\tau_0\xi\frac{1}{\rho}\int k_\nu Q_\nu dv = \frac{df}{d\eta}\xi\frac{\partial T}{\partial\xi},$$
$$T = T_0 \text{ for } \eta = 0,\ T = 1 \text{ for } \eta = \infty. \tag{14}$$

Here the temperature T is referred to the value in the incident flow; constant values are used for the product of the density ρ and thermal conductivity λ and also for the specific heat at constant pressure; the Prandtl number is one, and the Eckert number

is zero; $N = 2\delta T3_\infty\delta/\lambda$ is the radiative-conductive heat transfer criterion; the parameter $\tau_0 = k\delta$ characterizes the optical thickness of the boundary layer (k is the characteristic value of the radiation attenuation coefficient); $Q_\nu = (1 - \omega_\nu)(2n_\nu^2 J_\nu^0 - u_\nu)$ is the dimensionless divergence of the spectral radiation flux ($Q_\nu d\nu$ is referred to $2\delta T^4_\infty$); u_ν, J_ν^0 are the spectral radiation density and Planck function appropriately rendered dimensionless; the attenuation coefficient k_ν is referred to the characteristic value k; and the refractive index n_ν was taken as one.

The radiation energy density and flux were calculated in the planar-layer approximation [11], i.e., it was assumed that these quantities are completely determined by the corresponding temperature profile (and composition) in a given section of the boundary layer (value of ξ fixed), which is equivalent to solving the transport equation for the one-dimensional planar case. In other words, the solution to (10) was used to calculate the radiation term in (14).

The temperature profiles were calculated from the (13) inexplicit difference scheme. The temperature varies most rapidly near the plate, so we replaced η by the variable $v = a(1 - \exp(-b\eta))$ $(0 \le v \le 1)$; in the calculations, $a = 1.01$, $b = 0.25$, and the step in v was constant. I used a logarithmic scale for ξ with step $h = \Delta\ln\xi$. The conditions at the outer edge of the boundary layer were transferred to a finite large distance (this was done by choice of a in the expression for v).

The calculations were performed in the following sequence. For each section in the boundary layer, I used (10) to calculate the radiation flux and radiation energy density. Then I used (13) to derive the temperature distribution in the section.

Numerical results were obtained for a gray gas having attenuation coefficient proportional to the density with isotropic radiation scattering and with allowance for the anisotropy (for a two-term scattering indicatrix $\gamma(\mu, \mu') = 1 + a_1\mu\mu'$, $a_1 = 1$). The albedo ω was varied from 0 to 1 ($\omega = 0$; 0.3; 0.5; 0.8; 0.95 and 1). Results were obtained for a black plate, $T_0 = 0.1$, $N = 5$, $\tau_m = 1$ (this is the model considered in [3] for $\omega = 0$). The number of steps transverse to the boundary layer was $m = 20$, $h = 0.11729$ in the main calculations. Individual calculations for albedos of 0 and 1 were performed for twice that number of steps along the transverse to the boundary layer. The differences in temperature were less than 1%, but they attained several percent in the radiation density. Here ξ varied from 2×10^{-4} to about 900, which corresponds to optical thicknesses of the boundary layer from about 0.3 to about 500. For small ξ (optically transparent boundary layer), the errors in the radiation energy density were less than 1%. For $\xi > 27$ and $\omega = 0$, the errors in the radiation flux remained of the order of several percent at all points within the working region and became considerable at the plate, which is explained as follows. At such large distances from the leading edge of the plate, the boundary layer is optically dense, and one can use the radiative thermal conduction approximation to calculate the radiation energy flux. However, the corresponding difference approximation gives a large error at the plate because the step transverse to the boundary layer is too large due to the rapid temperature variation at the plate. That error in the radiation flux does not affect the temperature profile. The radiation flux at the plate can readily be refined. For $\omega = 1$, the error in the radiation flux is not increased at large ξ.

Figures 2-5 show the results for isotropic scattering with the above parameters. Figure 2 shows temperature profiles for $\omega = 0$ (solid lines) and individual temperature values for $\omega = 0.8$. For $\xi = 0$, the temperature profile is self-similar when one does not correct for the radiation (optical thickness of the boundary layer zero). For $\omega = 1$, that profile remains unchanged for all ξ. For $\xi = 892$, the temperature profiles are virtually identical for all the values of the albedo considered, apart from $\omega = 1$, and in fact coincide with the self-similar profile for the radiative thermal conduction approximation. For $\omega < 1$, the temperature profile alters as ξ increases from one self-similar solution (curve for $\xi = 0$) to the other (curve for sufficiently large ξ). The rate of alteration is dependent on the albedo.

Figure 3 shows the distribution of the radiation energy density u transverse to the boundary layer. As the optical thickness of the boundary layer increases, the u distribution tends to the equilibrium one defined by $u = 2T^4$. In Fig. 3, this is in fact the curve for $\xi = 892$, which is virtually the limiting curve for other $\omega < 1$. It is also clear that the equilibrium distribution is established earlier in the region adjoining the outer edge of the boundary layer.

Figure 4 shows the distribution with respect to η for the total heat flux $\hat{q}$ (curves 1 and 2) and the radiative heat flux q_r (curves 3 and 4), with the heat fluxes referred to σT_∞^4; $\xi = 0.12$ for curves 1 and 4 and $\xi = 3.2$ for curves 2 and 3. The total flux is equal to the sum of the radiative flux and the flux due to molecular thermal conduction. The solid lines give the flux distributions for $\omega = 0$ and the dashed ones for $\omega = 0.8$. The total heat flux has a maximum at the plate, while the radiative flux has one within the boundary layer. Near the plate is a region where the total flux hardly varies and there is redistribution of the heat transported by radiation and molecular thermal conduction. The points in Fig. 4 show the radiation energy fluxes calculated on the radiative thermal conduction approximation from the temperature profile for $\xi = 3.2$ ($\omega = 0$). That approximation applies for this ξ starting at a certain distance from the wall, but closer to the wall, the error increases, and the approximation is not suitable for calculating the radiative energy flux at the wall. However, the contribution from the radiative flux to the total flux is small near the wall, and the total flux to the plate is almost entirely formed by the temperature

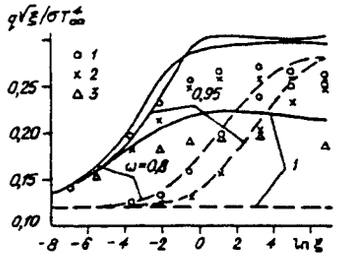

Fig. 8

profile close to the limiting one, so a numerical solution was obtained for $\xi > 3$ (with these parameters of ones close to them) that in a certain sense makes the radiative thermal conduction approximation applicable. It gives correct values for the radiation flux near the wall only when ξ becomes about 10^2, as can be seen from Fig. 5, which shows the distributions of the heat fluxes at the plate for various values of the albedo (the solid lines give the total flux q and the dashed ones the flux due to thermal conduction q_m). The molecular heat flux to the plate shows a behavior for all the ω other than 1 corresponding to shift in the solution from the self-similar one without radiation correction (for small ξ) to the self-similar one corresponding to the radiative thermal conduction approximation (for $\xi > 27$ with $\omega = 0$ and somewhat later for other values of ω). The total flux to the plate for $\omega \leq 0.8$ varies slightly with ω for $\xi < 1$ and is almost independent of ω for $\xi > 1$. The product $q\sqrt{\xi}$ tends asymptotically to a constant value for large ξ. The accuracy in calculating this value of the total flux is limited by the error in the difference approximation for the radiative thermal conduction at the plate.

Figures 6-8 give the results for linear anisotropic scattering with the above parameters. The solid lines in Fig. 6 show the temperature profiles for $\omega = 0.8$ and $a_1 = 1$ in various sections of the boundary layer. For comparison, points 1 and 2 show the temperatures in isotropic scattering (correspondingly in the sections $\xi = 0.62$ and 892, $\omega = 0.8$, and $a_1 = 0$). The temperature profile is independent of the radiation for $\xi = 0$. The maximum effect from the scattering anisotropy is seen on the limiting profile (for $\xi \to \infty$), and it is small with these parameters. Figure 7 shows the distribution of the radiation energy density u transverse to the boundary layer (symbols as in Fig. 6, $\omega = 0.8$). Here again, the largest effect from the scattering anisotropy occurs for large ξ. For $\xi = 892$, the relative change in the radiation density due to linear anisotropy is maximal near the plate (this is not evident in Fig. 7 because of the scale used).

Figure 8 gives the heat flux distributions along the plate due to molecular thermal conduction q_m and the total flux q (dashed and solid lines) with $a_1 = 1$ for the various albedos. Points 1-3 show the heat fluxes in isotropic scattering (they correspond to $\omega = 0.8$, 0.95, and 1) with $a_1 = 0$. The pair of points 1 for a single ξ represents the total heat flux (upper one) and the flux due to molecular thermal conduction (lower one) and similarly for points 2. The points 3 show only the values of the total heat flux. It is evident from Fig. 8 that the effects from the linear scattering anisotropy on the energy fluxes are considerable. The radiative thermal conduction approximation becomes correct somewhat later than in the case of isotropic scattering (at larger ξ). For $\xi > 100$ (optically thick boundary layer), the error in calculating the radiation flux to the plate becomes large, as for isotropic scattering, and the reason is the same.

Signs of computational instability occur for $0.8 \leq \omega < 1$ with isotropic or anisotropic scattering for $\xi > 10^3$ (optical thickness of the boundary layer greater than 600, and minimum transverse step greater than 5), which is evidently a consequence of the separate solution of the energy equation and (10) in each section of the layer for $r = 0$. No instability is observed for $\omega \leq 0.5$ and $\omega = 1$ (the calculations were performed up to $\xi \approx 10^4$). The run time with a BESM-6 computer was about 80 sec to calculate one model up to $\xi \approx 900$.

This numerical experiment shows that the proposed method is effective in solving stationary and nonstationary cases of radiative-conductive heat transfer in a planar layer on nets with any optical thickness for the step.

The above method of solving the transport equation also gives the angular distribution of the radiation intensity at any point in the layer as a series in Legendre polynomials if (6) has been solved for a sufficient number of intensity moments. The same method can be used in astrophysical treatments.

I am indebted to N. A. Rubtsov for a useful discussion on the results.

REFERENCES

1. Ya. B. Zel'dovich and Yu. P. Rayzer, The Physics of Shock Waves and High-Temperature Hydrodynamic Phenomena [in Russian], Fizmatgiz, Moscow (1963).
2. N. A. Rubtsov, Heat Transfer by Radiation in Continuous Media [in Russian], Nauka, Novosibirsk (1984).
3. V. P. Zamuraev, "A laminar boundary layer in a radiating and absorbing gas around a flat plate," Prikl. Mekh. Tekhn. Fiz., No. 3 (1964).
4. V. P. Zamuraev and R. I. Soloukhin, "Calculating the state of air behind a strong shock wave with allowance for radiation," in: Aerophysical Researches, Issue 5, Aspects of Gas Dynamics [in Russian], ITPM SO AN SSSR, Novosibirsk (1975).
5. V. P. Zamuraev, I. I. Maslennikova, and R. I. Soloukhin, "A study on radiative heat transfer behind shock waves in air by means of a multigroup averaging method," in: Heat and Mass Transfer in Strong Radiative and Convective Heating [in Russian], ITMO AN BSSR, Minsk (1977).
6. G. I. Marchuk, Methods in Computational Mathematics [in Russian], Nauka, Moscow (1977).
7. A. A. Charakhch'yan, "A numerical scheme for the transport equation on an optically coarse net," Zh. Vych. Mat. Mat. Fiz., **15**, No. 4 (1975).
8. V. I. Gryn', "Radiation transport calculation schemes," in: Radiating Gas Dynamics [in Russian], VTs AN SSSR, Moscow (1981).
9. V. V. Sobolev, Light Scattering in Planetary Atmosphere [in Russian], Nauka, Moscow (1972).
10. A. A. Charakhch'yan, "A numerical scheme for evolutionary treatments involving nonstationary radiation transport," Zh. Vych. Mat. Mat. Fiz., **18**, No. 2 (1978).
11. V. P. Zamuraev, "The error of the planar-layer approximation in describing radiation in a gray-gas boundary layer," Prikl. Mekh. Tekhn. Fiz., No. 1 (1965).
12. V. P. Zamuraev, "Calculating radiative-conductive heat transfer in a planar layer on a net with an arbitrary optical thickness step," Sub. Fiz.-Tekhn. Zh., No. 2 (1991).
13. V. P. Zamuraev, "Incorporating anisotropic scattering in calculating combined heat transfer in a planar layer on a net with an arbitrary optical thickness step," Sib. Fiz.-Tekhn. Zh., No. 4 (1991).
14. L. G. Loitsyanskii, Mechanics of Liquids and Gases [in Russian], Nauka, Moscow (1978).